The 12th International Symposium on Transport Phenomena and Dynamics of Rotating Machinery
Honolulu, Hawaii, February 17-22, 2008

ISROMAC12-2008-20074

EXPERIMENTAL AND NUMERICAL INVESTIGATIONS OF LEADING EDGE CAVITATION IN A HELICO-CENTRIFUGAL PUMP

D. Pierrat[1], L. Gros[1], G. Pintrand[1], B. Le Fur[1]
Ph. Gyomlai[2]

[1]CETIM, 74 Route de la Jonelière, BP 82617, 44326 Nantes Cedex 3 - France
Phone no: +33 (0).2.40.37.36.35
Email adress: daniel.pierrat@cetim.fr, laurent.gros@cetim.fr, guillaume.pintrand@cetim.fr, brigitte.leFur@cetim.fr,
[2]AREVA JSPM, 27 Rue de l'Industrie, 59 460 Jeumont - France
Phone no: +33 (0).3.27.69.91.28
Email adress: philippe.gyomlai@areva.com

ABSTRACT

In order to study the leading edge cavitation of the impeller of a single stage helico-centrifugal pump, a specific impeller with transparent shroud and a special casing with windows have been used as experimental test rig. The leading edge cavitation has been experimentally observed on the both sides of the impeller and the head drop measured for different operating conditions.

A CFD model for cavitation simulation has been investigated and compared to experimental results for 3 flowrates, ranging from 0.85 Q_n to 1.25 Q_n. The model uses a multiphase approach, based on a homogeneous model assumption. A truncated form of Rayleigh-Plesset equation is used as a source term for the inter-phase mass transfer. The cavitation figures are in a good agreement with the experimental ones for each flowrate.

INTRODUCTION

Cavitation phenomenon is still a limiting factor in the design of hydraulics turbomachines. When cavitation has enlarged, it is responsible for the noise and vibration generation, for the erosive damage with premature wear of the exposed surface, and for the loss of performance. Cavitation in turbomachines appears at operating conditions where the pressure locally drops to and below the vapour pressure.

CFD software has become essential to determine the set of operating conditions or modes that leads to cavitation. Such tools can be applied for two types of objectives. First, they are used for engineering and design purposes. The physical models are then relatively simple but assumptions are rather restrictive: indeed, they are based on a steady state approach and turbulent effects are most often modelled with the so-called eddy viscosity concept. Cavitation itself is modelled at a first order approximation of a vaporization model mainly based on the thermal and mechanical equilibrium assumption between liquid and vapor phases. Many works demonstrated that these models still give correct estimates of the loss efficiency and cavitation inception. Computation time is acceptable and compatible with industrial timeframes [Ait Bouziad et al., 2003, 2004][Ait Bouziad, 2006][Bakir et al., 2003, 2004][Catelan et al, 2005][Coutier et al, 2003, 2005][Luo et al, 2003][Mejri et al, 2006].

The second approach, which will not be developed in this work, is more focused on the transient aspects of the flow structure and of cavitation [Ait Bouziad, 2006][Athavale et al, 2002][Franc et al, 2004][Friedrichs et al, 2003][Hosangadi et al, 2005][Pouffary et al, 2003][Saito et al, 2003].

Most of recent works on the first approach concerns three-dimensional inducers [Ait Bouziad et al., 2003, 2004, 2006][Bakir et al., 2003, 2004][Coutier 2005], and in a lower proportion, centrifugal pumps [Catelan et al, 2005][Combes et al, 2000][Coutier et al, 2003][Luo et al, 2003][Hofman et al, 2001].

We consider in this current work the appearance of cavitation phenomena on helico-centrifugal pump. Experimental investigations have been lead on CETIM's ridge and numerical prediction of this behaviour has been investigated around nominal point. Two commercial CFD

packages were used to run numerical studies : CFX-TASCflow and ANSYS-CFX10. Results obtained are compared with experimental data such as Head, NPSH, efficiency and cavitation development on the blade. The choice of these two commercial software is justified by the fact that CFX-TASCflow has been a reference for turbomachinery applications [Hirschi et al, 1998][Ait Bouziad et al., 2003-2006][Bakir et al, 2003, 2004][Catelan 2005]. Though CFX10 uses the same discretization philosophy and velocity-pressure resolution technology [Scheuerer 2005][Mejri et al, 2006], it is not widely used yet.

The cavitation model used is the default one implemented in these codes. It is based on the so-called VOF (Volume of Fluid) model. In order to simulate the liquid/vapour mass transfer, a mass source term in the volume fraction transport equation is derived from a first order approximation of the Rayleigh-Plesset equation [Ait Bouziad, 2006][Bakir et al, 2004].

Major restrictions for design studies are realisation costs and delays. Velocity-pressure coupling method is particularly efficient to solve non-cavitating flows for turbomachinery. It enables the use of relatively fine grids without reaching prohibitive calculation costs, especially for conditions getting far from nominal ones. Nevertheless, the use of a cavitation model makes the Navier-Stokes equations behave in a highly non-linearly mode; this removes the possibility of working on such fine grids without a heavy and unrealistic CPU time for an engineering project. We intend to verify the consistency of results obtained within the framework of a standard engineering study requiring a reasonable calculation power. This current work presents the results of these investigations and develops the methodology for predicting cavitation in a pump.

NOMENCLATURE

Cp	[-]	Pressure coefficient $C_P = \frac{P - P_{ref}}{1/2\ \rho U_{in}^2}$
F2		SST modelling parameter
F^C, F^V	[-]	Cavitation modelling parameter
g	[m/s^2]	Acceleration due to gravity
H	[m]	Head $H = \frac{\Delta P_t}{\rho\, g}$
k	[m^2/s^2]	Turbulence Kinetic energy
$\dot{m}_l^C$	[kg/s]	Mass transfer between vapor and liquid, condensation process
$\dot{m}_l^V$	[kg/s]	Mass transfer between vapor and liquid, evaporation process
NPSH	[m]	Net Positive Suction Head $NPSH = \frac{P_{in} - P_{Sat}}{1/2\ \rho U_{in}^2} + \frac{u_{in}^2}{2g}$
P	[Pa]	Local static pressure
P_k	[m^2/s^3]	Turbulence model production term
P_V	[Pa]	Vapour saturation pressure
P_w	[kW]	Power
Q	[m^3/s]	Flow rate
Q_n	[m^3/s]	Nominal Flow rate
R	[m]	Wheel radius
r_0	[m]	Initial radius for nuclei
S	[s^{-1}]	Shear strain rate $S = \sqrt{2 S_{ij} S_{ij}}$
$\vec{T}$	[N.m]	Torque determined by the pressure and the viscous forces integration on the blades and impeller side walls
u_j	[m/s]	Cartesian velocity
x_j	[m]	Cartesian coordinate
y^+	[-]	Dimensionless wall distance
α	[-]	Volume fraction
ΔP_{Loss}	[Pa]	Loss $\Delta P_{Loss} = P_{total\ relatif,\ in} - P_{total\ relatif,\ out}$
ΔP_{total}	[Pa]	Total pressure variation $\Delta P_{total} = P_{total,\ in} - P_{total,\ out}$
ε	[m^2/s^3]	Turbulent eddy Dissipation
η_P	[-]	Efficiency based on pressure $\eta_P = \frac{\Delta P_{total}}{\Delta P_{total} - \Delta P_{Loss}}$
η_T	[-]	Efficiency based on torque $\eta_T = \frac{\Delta P_{total} Q}{\vec{T} \cdot \vec{\Omega}}$
μ_t	[Pa.s]	Mixture turbulent dynamic viscosity
ρ	[kg/m^3]	Density of mixture
σ	[-]	Cavitation number $\sigma = \frac{g\ NPSH}{\Omega^2 R^2}$
σ_b	[-]	Breakdown cavitation number corresponding to a fall of the total pressure
σ_c	[-]	Critical cavitation number corresponding to a drop of 3% of the total pressure variation
σ_d	[-]	Cavitation number corresponding to the appearance of the decrease of the total pressure
ω	[s^{-1}]	Dissipation per unit turbulence Kinetic energy
Ω	[rad/s]	Angular velocity
ψ	[-]	Specific energy tansferred to the flow $\psi = \frac{gH}{\Omega^2 R^2}$
ψ_t	[-]	Specific energy supplied by the whell $\psi_t = \frac{\vec{T}_t \cdot \vec{\Omega}}{\rho Q \Omega^2 R^2}$

Subscripts

g	Non-condensable gas
i,j	Cartesian tensor indices
in, out	Inlet, outlet boundaries
l	Liquid phase
v	Vapor phase

Acronyms

BJ	Barth & Jespersen Scheme (Convection scheme)
HR	High Resolution Scheme (Convection scheme)
LPS	Linear Profile Scheme (Convection scheme)
MPLS	Modified LPS (Convection scheme)
MUSCL	Monotonic Upstream-Centered Scheme for Conservation Laws (Convection scheme)
NAC	Numerical Advection Correction (Convection scheme)
PAC	Physical Advection Correction (Convection scheme)
SST	Shear Stress Transport Model (Eddy viscosity turbulence model)
SUDS	Skewed Upstream Differencing Scheme (Convection scheme)
RMS	Square root of the mean residual
RNG	Renormalization Group - k-ε RNG model (Eddy viscosity turbulence model)
TVD	Total Variational Diminishing (convection scheme)

EXPERIMENTAL INVESTIGATIONS

Test rig and Helico-centrifugal Pump design

A storage tank with a capacity of 15 m^3 is connected to an airdome. This airdome is a smaller tank that can be filled and emptied. A liquid ring vacuum pump is used to control the pressure at the free surface inside this tank. A 200 kW alternate current motor powered by a variable frequency controller is used to drive the tested pump. The rotational speed is measured using an optical sensor connected on a frequency meter (accuracy 0.3%). A motorized regulating valve allows the control of the flow rate. An electromagnetic flowmeter (accuracy 0.5%) located at the pump outlet, at a sufficient distance away from the pump exit, so that the flow is not too disturbed. Pressure levels are measured through transmeters (accuracy 0.3%). They are located at the inlet and outlet sections and give the average tip pressure on four pressure tapping. A temperature probe (accuracy 0.5%) is also used. One should note that the average temperature during the tests is below 28°C.

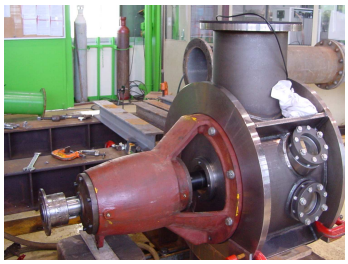

Figure 1: *Pump geometry.*

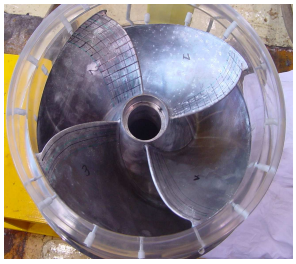

Figure 2: *Runner view*

A helico-centrifugal pump is a centrifugal pump, with a mixeted flow type impeller. Indeed, the main flow path is nor radial, nor axial but conical. The pump consists of a centrifugal four blade impeller in an axisymmetric volute with a radial outlet [Fig. 1, 2].

General Overview of experimental procedure

The impeller is equipped with a transparent acrylic shroud and the test section is optically accessible by windows in the side of casing for visual inspection of the cavitation [Fig1]. A stroboscopic light source was used for illumination of the optical observations. At each operating point, a picture is taken at the pressure side and the suction side of the blade. Thanks to the grid drawn on the blade, it is easy to sketch the cavitation gas pocket and its development during the test. The procedure for the experiments is the following: the impeller rotational speed is fixed at 1485 rpm. The flow rate is set to the operating value using the motorized control valve. It varies from 0.85 Q_n to 1.25 Q_n. The inlet pressure drop is obtained by the liquid vacuum pump.

A large range of flow rates was investigated around the nominal point of operation in non cavitating and cavitating conditions. For the cavitating cases, a level of static pressure equal to 7 bars prevents from the appearance of vapor. In cavitating conditions, the flow rate is kept constant, and the static pressure is decreased slowly to enhance vapour development in the impeller and reach the performance breakdown.

NUMERICAL AND PHYSICAL ASPECTS

Cavitation and turbulence modelling

To describe the cavitation process, one considers two phases made up of three components: non-condensable gas (g), vapour (v) and liquid (l). The relative quantity of each component can be described by a scalar volume fraction: α_g for incondensable, α_v vapour and α_l liquid with a sum equal to unity. The non-condensable has an important influence on cavitation, especially on cavitation inception, which is related to the tension surface strength of the liquid. Generally in standard cavitation models, it represents the nuclei, in particular in those implemented in CFX-TASCflow and CFX10. The non-condensable component is assumed to be a gas (air) and its density can be determined from an ideal gas equation of state using local pressure and temperature. The presence of non-condensable gas is accounted for by assuming it to be well premixed in the liquid phase. In this case, two mass fractions of non-condensable and liquid can be combined and treated as one (CFX-TASCflow). The incondensable volume fraction is generally lower than 10^{-3} and it can thus be taken in account only in the mechanism of vaporization (CFX10). If the volume fraction is higher, it is better to consider a variable mass fraction [Singhal et al., 2004].

In the current models of cavitation, there are two phases: the liquid (or pure substance mixture: liquid + non-condensable) and vapour are assumed to be mechanical equilibrium (no interphase slip). A homogeneous mixture multiphase can be used with a single set of momentum equations. One volume-fraction equation is retained to solve for the distribution of two phases in the flow. The non-equilibrium description of the dynamics of phase change is schematized into source term which is implemented through a volume fraction equation. This homogeneous multiphase approach makes it possible to take into account cavitation as an interphase mass transfer process. One can thus use volume fluxes rather than mass fluxes. Volume fluxes are continuous at the interface, what facilitates the numerical processing.

This model differs from the free-surface method standard where a bubbly mixture and pure vapour zone are clearly separated by the moving interface [Hirchi et al, 1998] [Kawamura et al, 2003]. In the common VOF transport model, no attempt is made to model a distinct liquid/vapour interface. The volume fraction field may vary continuously from 0 to 1 in the cavitation zone covering many grid elements. And visualising the development of cavitation pockets is possible through an iso-surface at 10% of vapor in the mixture or in the liquid [Ait Bouziad et al, 2003][Bakir et al, 2003].

A source term into a volume-of-fluid equation [Eq 1] is provided by a Rayleigh-Plesset equation governing bubble dynamics. This model assumes a thermal equilibrium, on a zero slip velocity bubble and without bubble interactions. A first order approximation explicitly gives the equation of the rate [Eq 2][Eq 3] controlling the vapour generation (vaporization) / destruction (condensation), neglecting the viscous damping, the surface tension and initial bubble acceleration effects. Mass exchange between vapour and liquid (or mixture: Liquid + Non-condensable) is given by the equations below:

$$\frac{\partial}{\partial t}\left(\rho_l \alpha_l\right) + \frac{\partial}{\partial x_j}\left(\rho_l u_j \alpha_l\right) = \dot{m}_l^C - \dot{m}_l^V \quad \text{[Eq 1]}$$

with

During vaporization:

$$\dot{m}_l^V = F^V \frac{3\alpha_g \alpha_l \rho_v}{r_0}\sqrt{\frac{2}{3}\max\left(\frac{P_v - P}{\rho_l}, 0\right)} \quad \text{[Eq 2]}$$

During condensation:

$$\dot{m}_l^C = F^C \frac{3(1-\alpha_l)\rho_v}{r_0}\sqrt{\frac{2}{3}\max\left(\frac{P - P_v}{\rho_l}, 0\right)} \quad \text{[Eq 3]}$$

In this model, the bubble pressure or rather phase change threshold pressure is assumed to be equal to the vapour saturation pressure in absence of dissolved gas. This value is evaluated at the temperature of the surrounding liquid. It is possible at this stage to simply take into account the influence of the turbulence by increasing the pressure threshold by the values of the turbulent pressure fluctuations [Ait Bouziad 2006][Yang et al, 2005]. This option available in CFX10 was not tested in presented works.

The non-condensable gases with a volume fraction (α_g) are assumed to be present as spherical bubbles which provide nucleation sites. The values generally taken for α_g are: 5.10^{-7} [Catelan et al, 2005], 10^{-5} [Ait Bouziad et al, 2003], and 5.10^{-4} [Scheuerer, 2005][Mejri et al, 2006]. Extreme values have been tested here. These authors assume an initial radius for the nuclei (r_0) equal to 10^{-6}m, this value has been retained. The constants F^V and F^C are introduced to account for the fact that the vaporization and condensation processes have different times scales. Their values, $F^V = 0.01$ and $F^C = 50$ are derived from numerical testing, using experimental data of the cavitating flow on a two-dimensional hydrofoil [Ait Bouziad et al, 2003][Bakir et al, 2004].

The vapour density can be calculated using an ideal gas relation. For a low speed flow, the vapour density can be assumed as a constant value, estimated at the vapour pressure and fluid temperature. In this work, the fluid temperature is also considered constant at a typical value observed during the experiments, T=300 K.

In spite of computing power increase, the Reynolds-averaged Navier-Stokes (so-called RANS) equations are always mainly used for the 3D problems and particularly Eddy Viscosity Models [Hanjalic, 2005]. Eddy Viscosity Model are often used in the numerical study of cavitation phenomena in turbomachines: k-ε standard [Ait Bouziad et al, 2004][Bakir et al, 2003][Mejri et al, 2006], k-ε-RNG variant [Bakir et al, 2004][Coutier-Delgosha et al, 2003], or k-ω formulation [Kawamura 2003][Basuki et al, 2003].

Concerning the k-ε-RNG model, we observed its tendency to largely depend on mesh distortion. It was not retained. The ω equation in the k-ω formulation has significant advantages near the surface and accurately predicts the turbulent length scale in adverse pressure gradient flows, leading to improved pressure and wall shear stress. This model has a very simple Low-Reynolds formulation which does not need additional non-linear wall damping terms. A Dirichlet boundary condition for ω correctly describes a linear sublayer, but requires a high grid density : $y^+ < 2$ [Wilcox, 1993] In order to avoid this constraint on the near wall mesh, Menter proposed an automatic near-wall treatment which can shift gradually between from a viscous sublayer formulation to the standard wall function (Automatic Wall in vocable CFX) [AEA, 2002]. But a problem with the k-ω model, is its strong sensitivity to free-stream conditions [Menter, 1992]. However, this behaviour does not seem to appear for studies on unsteady flows [Kawamura et al, 2003][Mejri et al, 2006]. In order to solve this problem, a blending

between the k-ω model near the walls and the k-ε model in the outer region was developed by Menter [Menter, 1993]. If this model combines the advantages of the k-ω and the k-ε model, it still fails to predict the onset and amount of flow separation from smooth walls due to the over-prediction of the eddy-viscosity. An additional feature was proposed by Menter [Menter, 1994, 1996] consisting in the introduction of an upper limit for the turbulent shear stress in the boundary layer in order to avoid excessive shear-stress levels predicted with standard Eddy Viscosity model:

$$\mu_t = \rho \frac{0.31k}{\max(0.31\omega, F_2 \cdot S)} \qquad \text{[Eq 4]}$$

S is the shear strain rate and F_2 is a blending function which restricts the limiter to the wall boundary layer. This limiter gives a non-linear behaviour to turbulent viscosity, which enables the SST model to be efficient to simulate unsteady phenomena. However, in the case of cavitation, the turbulent dissipation can be over-estimated in the rear part of the cavitation sheet. This effect can artificially stabilize the cavitation zone, thus removing its transient. To correct this effect, Coutier [Basuki et al, 2003[Coutier et al, 2003][Scheuerer, 2005] gives a simple modification on the turbulent viscosity. The density ρ is replaced by a function which is equal to ρ_v or ρ_l in the regions containing respectively pure vapour or pure liquid (ρ_m if non-condensable is present). This function decreases quickly toward ρ_v for intermediate void ratios. However, this modification is efficient only if the mesh is strongly refined, which makes it applicable to only unsteady 2D cases. Menter [Menter 1993][AEA, 2002] also proposed a limiter to the production rate of turbulent kinetic energy in order to remove the build-up of turbulence in stagnation regions of airfoils or blades. This limits the imbalance between production and dissipation to a certain level (10 by default):

$$P_k = \min\left(\frac{\mu_t}{\rho} S^2, 10 \cdot \varepsilon\right) \qquad \text{[Eq 5]}$$

For adverse pressure gradient, the SST model gives better results than the k-ε model. In 3D cases, this model requires too fine a grid which makes it inapplicable on turbomachinery cases. This explains why the one does not observe large differences in the solutions given by both models [Asuage et al, 2005]. In this work, we will compare the two models but only for non-cavitating cases.

Computational methodology

The commercial packages CFX-TASCflow and ANSYS-CFX10 solve the Reynolds-averaged Navier-Stokes (RANS) equations with a finite-volume/finite-element method [Aea, 2002][Ansys, 2005][Raw, 1985][Schneider et al, 1987]. The solution of the velocity-pressure system is based on a fully coupled approach. The linearized equations of momentum and continuity are solved simultaneously with an Algebraic Multigrid method based on the Additive Correction Multigrid strategy [Hutchinson et al, 1986, 1988][Ruge et al., 1987]. The relaxation scheme used in the W cycle is the Incomplete Lower Upper Factorization Solver. Solving the fully coupled form of the equations (mass and momentum) ensures one fully benefits from the multigrid speed-up of the pressure operator [Ferry et al., 1991][Gros et al, 2006]. The coupling between the different velocity components (the Coriolis effect) is also solved in a coupled manner. The implementation of this strategy in CFX-TASCflow and ANSYS-CFX has been found to be very robust and efficient in predicting swirl flow in turbomachinery [Bache et al, 1990][Raw, 1996].

CFX-TASCflow is a three dimensional structured mesh code while ANSYS-CFX10 is a three dimensional unstructured mesh code. However, multiblock structured meshes are used here with the two codes. These meshes are generated with CFX-TurboGrid (V.1.6.03) a specific mesher dedicated to turbomachinery. Multiblock structured mesh is still widely used and preferred by CFD analysts for it is the best suited for turbomachinery applications. Indeed, it allows the best quality mesh in the wheel region while keeping a reasonable number of cells. It is important to note that the so-called CV-FEM method (control volume/finite-element method) remains efficient on hexahedral meshes while the use of tetrahedral meshes tends to degrade its efficiency. One should note that the construction of the dual control volume (based on the aggregation of neighbouring tetrahedral) is done only within the solver stage: it is therefore difficult to gauge the quality of the resulting polyhedral mesh. Because of this two-step method, in some cases, smoothing the tetrahedral mesh can highly degrade the local quality of the polyhedral meshes.

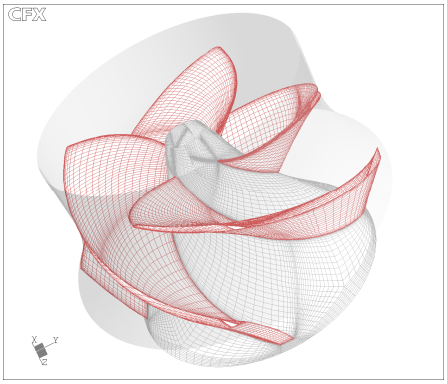

Figure 3: *Mesh visualisation*

A grid dependency study is first carried out on a non-cavitating flow. Selected final mesh consists for a single blade passage of 220 000 nodes. Specific cell thickness progression laws in the meridian, hub-to-shroud and blade to blade directions are applied to ensure good grid quality: near wall orthogonality is enforced and slightly skewed

mesh is observed in the remainder of the domain with a maximum element aspect ratio lower than 1000; cells evolution factor is lower than 1.25 [Fig. 3].

The numerical prediction of cavitating flows is a difficult problem and often requires small time steps to control the non-linearity generated by the model (Cf next paragraph). To keep the CPU time reasonable, the model includes only the wheel. The computing domain to predict to cavitating flow consists in a single blade to blade passage. The boundary conditions used are total pressure at the inlet and mass flow at the outlet. The connection between the periodic faces is made by periodic connections.

Experiments results include measures of pressure values at the pump inlet and casing outlet. It is therefore necessary to also measure the global values of the pump itself in order to derive the pressure drop due to the volute. The CFD results on the wheel only can then be compared to the experiments. The prediction of the pump global values has been performed in a non cavitating regime. The whole wheel was meshed (4 x 220 000 nodes). The volute was meshed with ICEM CFD Hexa. The whole pump mesh consists of 1.2 million nodes. The flow a through an impeller and the volute is considered in steady-state-regime, in which the impeller is solving in a rotating frame and the volute is solved in the stationary frame. The two frames of reference connect to each other in such a way that they each have a fixed relative position throughout the calculation, with the frame transformation along a sliding interface (Frozen-Rotor interface)[AEA, 2002].

Calculating accurately the convective fluxes is essential for the reliability of the solution. In the present work, refining the mesh in order to use a second order Central Differencing Scheme (CDS) – for which one note considerable convergence oscillation – was not possible. Though it indisputably brings stability to the convergence, the Upwind Differencing Scheme (UDS) is not accurate enough to allow a safe and correct interpretation of the results. This lack of precision is particularly underlined by this symptom: consider the efficiencies, on the one hand based on the total pressure and relative pressure of the wheel alone (η_P), and other based on the power calculations (η_T); when the two figures are different from a certain difference, one can conclude to an accuracy issue. In our case, we observe, with UDS scheme, a difference far above 20% even on a finer mesh of 220 000 nodes for the one blade passage.

Results are affected by the characteristics of the numerical scheme employed in calculating the convective flux. The interpolation scheme should able of reducing the errors arising from numerical diffusion in both the streamwise and cross-stream directions. Streamwise diffusion occurs when gradients parallel to the flow exist for a convected variable. On the other hand, cross-stream diffusion occurs in a multidimensional flow when gradients in a convected variable exist perpendicularly to the flow. So as to improve interpolation schemes precision of the convected variable at a defined point, two different philosophies are employed by the two tested codes. It appears important to briefly precise the characteristics of these schemes so as to ease the interpretation of solvers behaviour. In CFX-TASCflow, the convected variable is composed of two terms at the integration point, formulated in the streamwise direction: value of the convected variable on the streamline upstream, and correction required to account for the variation between this evaluation and the value at the integration point. This correction, which reduces errors in the streamwise direction, considers interactions between diffusion, source terms and, when the variable is a velocity component, pressure gradient and the Coriolis term in a rotating frame [AEA, 2002][Raw, 1985]. For stability reasons, Skewed Upstream technique introduced by Raithby [Raithby, 1976], depending on a scaled upwind velocity, is introduced in this Physical Advection Correction.

The first term only includes values of the upstream nodes surrounding a defined point (Skewed Upstream Differencing Scheme), which ensures a relative stability [AEA, 2002][Schneider et al., 1986]. A trilinear interpolation of the nodal values, Linear Profile (LPS) enables to reduce errors in cross-stream directions, thus ensuring a second order precision for the scheme (LPS+PAC) [AEA, 2002] [Raw, 1985] Despite its robustness, this scheme can generate unphysical wiggles. To diminish this risk, only the closest upwind nodes of the element are used for the approximation (Modified LPS). But in this case, MLPS is only first order in the transverse direction. Moreover, PAC correction does not represent a full physical scheme in a multidimensional flow because interpolation along element edge is necessary!

Nevertheless, the MPLS scheme does not guarantee an unconditional stability of the convective operator. In CFX-TASCflow, an other scheme; more stable but less accurate than MPLS, guarantees positive coefficients: Mass Weighted SUDS: [AEA, 2002][Schneider et al., 1986]. This scheme is generally applied to critical variables such as the volume fraction. Transposition of this SUDS philosophy to unstructured grids is not easy. In a unstructured mesh code, the implementation of convective schemes is preferred such as a deferred correction to the first order Upwind Scheme (Numerical Advection Correction). The correction can be viewed as an anti-diffusive flux added to the Upwind Scheme. The degree of 'anti-diffusiveness' is controlled by a parameter (β): 0-upwind, 1-High order upwind. A High-order Upwind scheme suffers from a lack of boundedness: it tends to give rise to unphysical oscillations. This numerical dispersion can be avoided by using TVD schemes (Total Variational Diminishing). Although they are widely spread on

structured mesh, it is tricky to apply them to unstructured grids, specifically because of the difficulty in implementing a monotonicity criterion that relies on directional next-neighbour information, which is missing in unstructured grids. To circumvent this difficulty, unstructured mesh code uses Barth and Jespersen method that involves an explicit reconstruction of the flux at cell faces and enforces a monotonicity criterion less restrictive than the one used on classic TVD approach [Barth et al, 1989][Barth, 2003].

Regardless of implementation difficulties, it should be noted that a simple transcription of one-dimensional TVD approach to 3D case would be excessively restrictive and would lead a drastic fall of scheme precision, due to a systematic and unwanted switch to the first order. While the Barth and Jespersen [BJ] scheme is not TVD based, it can be shown to be equivalent to the TVD_MUSCL in one dimension only (Monotonic Upstream-Centered Scheme for Conservation Laws) [Darwish et al, 2003]. In the case of an inactive boundedness criterion, the BJ scheme is almost equal to the Fromm Scheme, which is an arithmetic mean of Second Order Upwinding and Central difference.

COMMENTS OF NUMERICAL ADJUSTMENTS AND INFLUENCE OF TURBULENCE MODEL

Interpolation schemes

Non-Cavitating flow

Tests on mesh density influence and convective numerical schemes were performed on the non-cavitating case with the impeller only. Actually, in the case {impeller + volute}, the comparison between η_P and η_T would not be correct. For all numerical predictions of non-cavitating flows, the maximum values of residuals are kept below 10^{-4}, which leads in turn to RMS values of residuals below 10^{-6} for all conservation equations. The combination of MPLS & PAC, which is not second order accurate in the transverse direction, keeps the coupled solver efficiency without damaging the global values estimation.

If edge element interpolation is fully used (LPS + PAC), the accuracy is improved but requires under-relaxation and the number of iterations increases while moving away from the nominal point. It explains why (MPLS + PAC) scheme is chosen for the turbomachinery calculations in SUDS approach. It should be noticed that this strategy requires a good quality regular mesh with a smooth expansion, so as to reach an optimum precision level.

The activation of a high order scheme based on NAC approach, leads to convergence only if the monotonicity criterion is applied on its anti-diffusiveness part (BJ_MUSCL). The picture on the right [Fig. 4] shows the normalized limiter for momentum quantities. Although the scheme precision is deteriorated near walls, the gap between efficiencies remains reasonable, lower than those obtained with (MPLS + PAC) schemes [Table 1]. These results confirm that in this region, the omission of gradients of convected variables, existing in the direction perpendicular to the flow (MPLS), penalizes more than a local reduction of the anti-diffusiveness part of the High Resolution scheme. Nevertheless, the use of High resolution scheme requires a computational power higher than the one observed when LPS scheme is activated. This could be a consequence of the BJ_MUSCL scheme instabilities. Indeed, based on the analogy between the Barth & Jespersen formulations and the MUSCL scheme, the gradients of convected variables in the solver iterative process may evolve in the area of slope sign change of the characteristic function, which leads to oscillations of the slope limiter [Darwish et al, 2003]. In critical cases, this can lead to a significant rise in calculation time, compared to CFX-TASCflow [Table 1].

Schemes	**Number of iterations**	$\frac{\lvert\eta_P-\eta_T\rvert}{\min(\eta_P,\eta_T)}$	*Time step*
MLPS+PAC	100	2%	0.3/Ω
LPS+PAC	300	0.1%	0.1/Ω
BJ_*MUSCL*	350	0.4%	0.1/Ω
BJ_*Fromm*	No converge		

Table 1*: Schemes – Accuracy and computational effort*

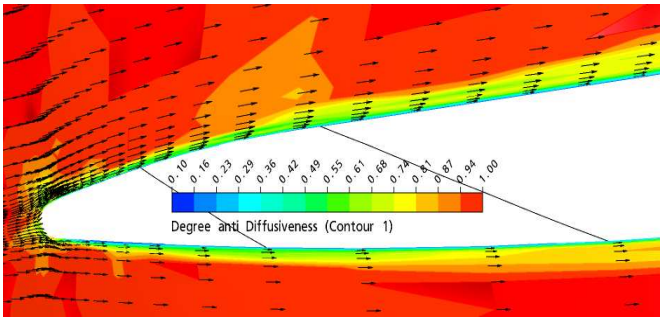

Figure 4: *Degree of anti-diffusiveness of scheme Non-cavitating case - $Q=Q_n$*

Cavitating Flow

The numerical prediction of cavitating flows is a difficult problem. The behaviour of the Navier-Stokes equations is highly non-linear. Actually, the vaporization process can lead to large spatial gradients in the flow mixture density field. This density ratio can bring a lot of difficulties for the convergence, even with an approach where velocity and pressure are solved simultaneously. Hutchinson gave more precisions on Bakir's work [Aea, 2002][Bakir, 2004]: numerical adjustments are necessary to make the solver stable. Its performances remain thus correct even for the higher density ratio. Among these adjustments, in CFX-TASCflow, one can note the enhancement that consists in switching from second order to first order discretization of the momentum equations in

regions where the mixture density varies dramatically. However, this adjustment tends to degrade the accuracy of the transient solution. Indeed, the numerical diffusion would remove this enhancement brought by the weighting operations of the turbulent viscosity. Moreover, applying the second order scheme (LPS + PAC) for the momentum equations only in the regions of pure fluid makes the solver highly unstable. The simulations could be completed only when the scheme (MPLS + PAC) was used.

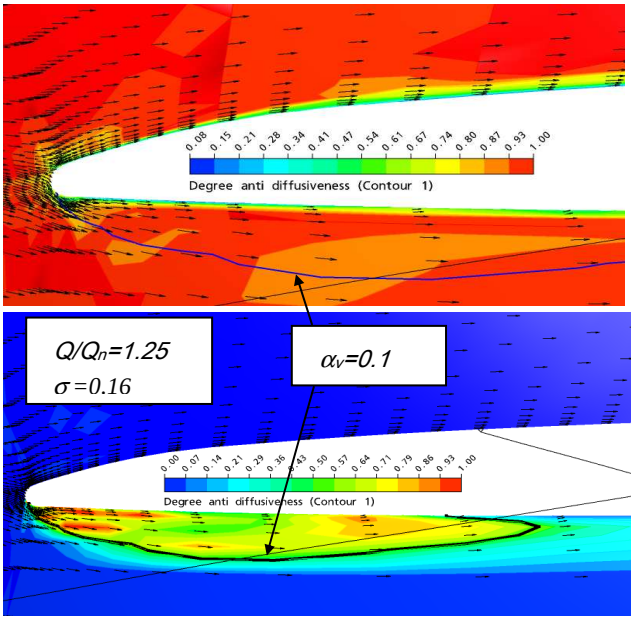

Figure 5: *Degree of anti-diffusiveness of momentum quantities (Top) and volume fraction (Down)*

In areas of high velocity gradients, the robustness of the solution in BJ_MUSCL approach was maintained thanks to the flux limiter in the interpolation scheme of the advected velocities [Fig. 5]. The discretization of the advected volume fraction also uses a TVD scheme for which the flux limiter ensures stability on zones of volume fraction gradients. This scheme is only forced to first upwind differencing (UDS) in zones where the liquid is dominant [Fig.5] and not in the entire domain as this is the case in CFX-TASCflow.

Compared to the (MPLS + PAC) scheme, the use of BJ_MUSCL is more demanding in computation time for higher cavitation numbers. As this number drops, the computation efforts become quite similar for both codes. Let us illustrate this point: for a cavitation number of σ = 0.18 ($Q = 1.25Q_n$), 2000 iterations are required for both solvers to converge to the same levels of residuals. However, one can note that in CFX10, for cavitation numbers below critical values (for instance σ = 0.15 at the nominal point), the maximum values of the residuals for the momentum oscillates around the average value 10^{-3}. This prevents us from using only the residuals as convergence criteria. Therefore, at these critical values, we also monitor the head values. The simulations are considered as correctly converged when the standard deviation of the head mean value is below 2.10^{-4} m.

More generally, for each operating point, an incompressible solution is first computed without activating the cavitation model. From this non-cavitating solution, the cavitating model is turned on while the total pressure at the inlet is decreased by a constant step of 1 bar. Near the drop zone, this step is reduced by a factor 10 to 100 in order to overcome the high instability due to the non-linear behaviour of the cavitation model. The required time for these computations of a whole one head drop curve (~32 points) is about 15 days on a 2.8GHz two processor HP Workstation. Despite the degradation of accuracy in the convective schemes (especially in the zone of cavitations) may lead us to the conclusion that CFX-TASCflow is more robust, one observes similar computational efforts for both to reproduce the whole head drop curve. The non-linearities due to the cavitation models are therefore the major factor of instability for CFD solvers.

Turbulence model

Y+ maps show that mesh density is inadequate near walls to benefit from the Low-Reynolds behaviour of k-ω to make sure the Dirichlet condition model closure conditions on ω correctly applies, the first point must indeed be located at a wall distance verifying y^+=2, and the number of points in the sublayer has to be sufficient so as to reach the elliptical behaviour of the ω equation [Fig. 6].

In the current mesh (220.000 nodes for a single blade passage), the wall distance of the first point corresponds to 0.05% of the blade-to-blade width. This distance should be shortened by a factor 50 to benefit from the Low-Reynolds behaviour of k-ω. Considering that mesh expansion cannot exceed a certain value, in particular for CFX10 because of HR schemes corrective terms based on a node-centred formulation, and that in other directions, overstretched cells would generate some numerical difficulties, this grid thinness would lead to a prohibitive number of elements.

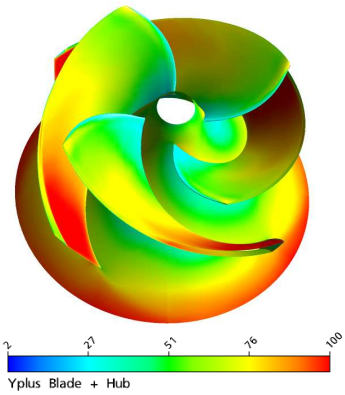

Figure 6: *Hub and blades Field of Y^+*

The ability of k-ω model to prescribe a detachment in presence of an adverse pressure gradient is partly caused by the lack in the ω equation of a cross-diffusion term [Menter, 1993]; this term though appears in the k-ω formulation of the k-ε

model. Now, this one essentially acts in a zone of the internal layer. As a conclusion, a too coarse mesh near the wall can explain the similarities often observed between results given by k-ω or k-ε models, or a hybrid formulation (so-called Base-Line model [BSL]).

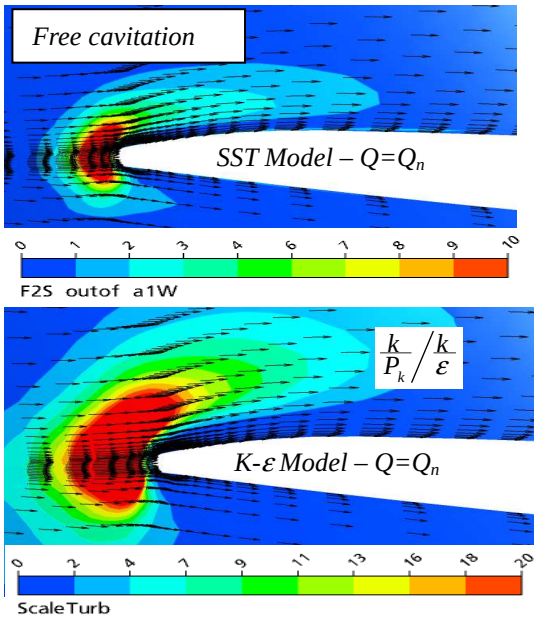

Figure 7: *characteristic scales of SST model*
Top : $F_2S/(0.31\omega)$ – Bottom : P_k/ε

In our case, the specific terms of the SST model [Eq 10][Eq 11] might modify the solution. The ratio between the production time scale and the dissipation one indicates that turbulence production is only clipped in the stagnation regions on the blades. However, this effect remains limited on the turbulent kinetic energy level [Fig. 7]. Similarly, the limiter on the viscosity practically acts only in this zone and does not significantly influence the downstream velocity field.

These observations confirm in a general way the similarity of solutions obtained with k-ω and SST model [Asuage et al, 2005]. In the present case and for the different operating points ($0.85Q_n$, Q_n, $1.25Q_n$), we notice a gap lower than 0.1% for the efficiency and below 0.5% for other global values (Head, Torque, Power). One should note that this remains true only for operating conditions close to the nominal point. For a partial load close to nominal flow rate, the flux is not aligned with the blade profile and generates a consequent flow deformation, so it legitimizes the use of the SST model or other models such as the k-ε realizable model. In this case, the mesh should be drastically finer in the leading edge zone, where the vorticity will be strong. Unfortunately, this leads to a larger mesh: the computation time will rise as at these regimes, unsteady flow behaviours can appear.

The previous analysis on the influence of the turbulence model (k-ε, k-ω, SST) on the results was performed for the non-cavitating cases. It can also be translated to the cavitating cases. Indeed, one observes that only the limiters specific to the SST models would be activated. But they would only be active in the vicinity of the leading edge: this does not fundamentally change the standard k-ε model turbulent scales downstream of this zone [Fig. 8]. Besides, the near wall regions mesh density is not sufficient to benefit from the k-ω formulation. Therefore, the turbulent phenomena are reproduced only through standard wall functions. The tests did not show large differences of the global values (<1%) between the k-epsilon and k-omega SST models.

For non-cavitating flows, the mesh can be refined (although the resulting mesh is too fine to be used in industrial contexts), which permits the SST model to correctly predict the global structures along the blade and more the specifically on the suction side. For cavitating cases, this is not the case: indeed, the interaction between turbulence and cavitation remains complex to model using classical modelling. Attempts were done by several authors using two-equation models to predict the cavitation instabilities. But then the meshes are particularly fine, which limits their applicability to 2D domains. Results are correct but the process requires a validation step [Ait Bouziad, 2006][Bazuki et al, 2003][Coutier et al, 2003, 2005][Reboud et al, 2003]. In our case, the mesh density is consistent with the values observed in most of the 3D cases studies in literature but does not allow a such adaptation.

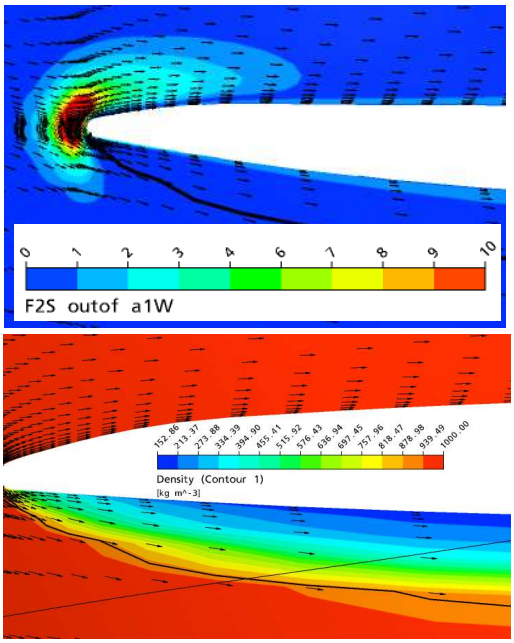

F
igure 8: *Q/Q_n= 1.25 – σ=0.16 :*
Top: $F_2S/(0.31\omega)$ - Bottom: Density

RESULTS

Non-cavitating flow

The tests performed alone impeller and the impeller with its volute (differentiation schemes, turbulence models) revealed that the precision of numerical schemes have a larger influence than the turbulence models (k-ε, k-ω, SST).

The use of the second order non monotonic scheme (LPS + PAC) makes it difficult to converge in the case {wheel + volute}. This convergence is not even obtained when activating the cavitation model. Using the BJ_MUSCL scheme ensures an acceptable convergence in both regimes. The analysis on the impeller alone indicates LPS + PAC is less accurate: the differences are in the order of 1.5% for the torque values and 1% for the other values (head and efficiency). However, when the whole pump is simulated, these differences are below 0.6%. Both codes give quite similar results on the three simulated points.

The table [Table 2] below compares the results obtained for the three operating modes considered for the {impeller + volute} case obtained with CFX10. The results for the sole wheel are also present :$0.85Q_n$ and Q_n. The specific energy supplied by the impeller to the flow and the corresponding energy coefficient, are given by:

$$E_t = \frac{\vec{T}_t \cdot \vec{\Omega}}{\rho Q} \text{ and } \psi_t = \frac{E_t}{\Omega^2 R^2} \qquad \text{[Eq 6]}$$

Where $\vec{\Omega}$ is the angular rotation speed and $\vec{T}_t$ is a torque determined by the pressure and the viscous forces integrations on the blades and impeller side walls [Hirschi et al 1997].

The energy transferred to the flow, and the corresponding specific energy coefficient (Pressure coefficient), are calculated using the hydraulic energy difference between the low pressure and the high pressure section of the considered element [Hirschi et al 1997][Bakir et al, 2004].

$$E = gH \text{ and } \psi = \frac{E}{\Omega^2 R^2} \qquad \text{[Eq 7]}$$

Where H is head of considered element : the wheel alone or the entire pump.

The loss can be evaluated by comparing these coefficients. One should observe the important losses caused by the volute. This is due to its special shape that facilitates the visualization of cavitation pockets: the sharp angles are likely to trigger strong local eddies [Fig. 9]. This table also points out that the nominal point would correspond to the partial flow $0.85Q_n$. Q_n which is the point of design corresponds rather to an overload condition. This discrepancy was confirmed during the testing [Fig. 10]. Values obtained in experiments and by computation are in excellent agreement.

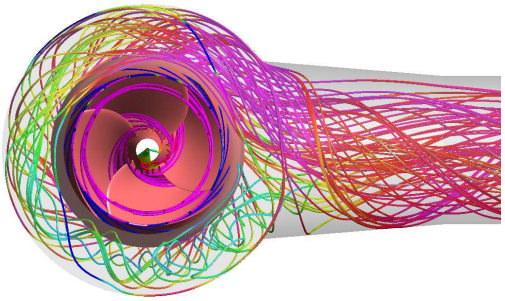

Figure 9: *Structure of the flow in the volute - Free cavitation*

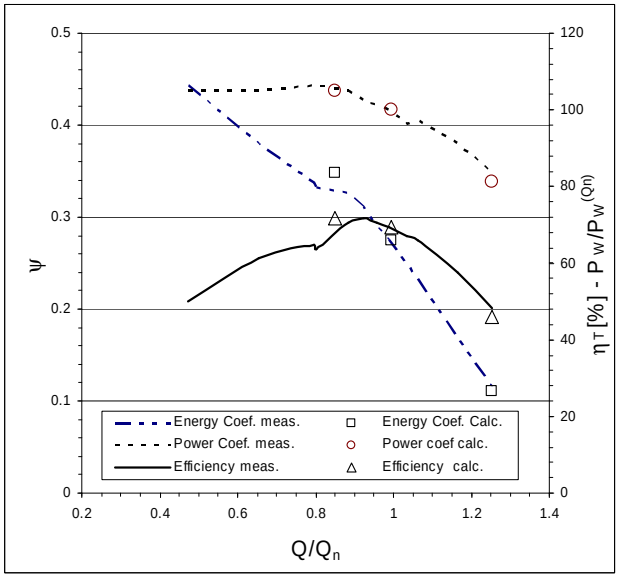

Figure 10: *Cavitation Free - Comparison Experimental results – Numerical Prediction: ψ (Energy Coef.), $P_w/P_w^{(Qn)}$) (Power Coef)˙,η_P (Efficiency)*

Model : Wheel + volute					Model:impeller alone		
		$0.85Q_n$	Q_n	$1.25Q_n$		$0.85Q_n$	Q_n
Wheel alone	ψ	0.450	0.361	0.213	ψ	0.437	0.356
	ψ_t	0.491	0.401	0.255	ψ_t	0.474	0.381
	η_T	0.915	0.903	0.835	η_T	0.921	0.92
Pump	ψ	0.353	0.277	0.117			
	η_T	0.720	0.693	0.457			

Table 2: *Non cavitating flow – Performance*

The energy transferred through the impeller alone (ψ_t) is lower than the energy transferred to the whole model (5%). The ratio on each blade of the specific energy on the average value shows the effect of the volute of the energy transfer mechanism in the pump. The influence remains mostly localized at the blade pressure side at the impeller

exit. It has no significant effect on the pressure along the suction side [Fig. 11]. This indicates that for number of cavitations beyond the critical values corresponding to the heat drop, the influence of the volute is does not play a major role in the impeller inception of cavitation, thus legitimizing the fact to consider as a first approach the impeller alone.

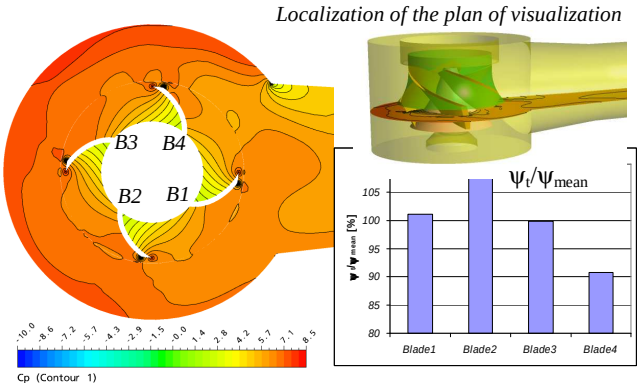

Figure 11: *influence volute on the pressure field and on the torque (ψ_t) of each blade*

Cavitating flow

None of the two codes revealed significant differences in their behaviour or in the global values predicted for the nominal points. For both codes, one can note the same convergence issues near the numerical critical cavitation number values that correspond to the drop of performance.

The specific energy coefficient ψ [Eq5] calculated is plotted as a function of the cavitation number σ [Fig. 12]. The experimental values are also plotted on the same graph. The agreement between experimental results and numerical predictions is quite acceptable. But the critical cavitation number (σ_c) is systematically underestimated by the simulation. The numerical head-drop occurs with lower values of cavitation number and is steeper than the experimental curve. What prevents from differentiating breakdown number (σ_b) from critical cavitation number (σ_c).This gap may be due to the facts that the pocket instabilities were not accounted in a cavitation model. It can also be attributed to the selected values for the empirical coefficients of vaporization and condensation terms, to the restrictions of the turbulence model, and to the too coarse mesh [Mejri, 2006]. One will note that in our case, at critical values of σ, the leakage flow was not accounted as the impeller alone was considered. Moreover, at these regimes, the influence of the volute may not be negligible in the phenomena [Hirschi, 1997]. One may also observe a difference at the beginning of performance drop. At partial flow, the experimental curve starts to drop at a higher cavitation number. This drop is not predicted, and on the contrary, a slight increase in the head is computed. At nominal point, we observe experimentally that the start of this drop is closer to the value of breakdown cavitation number than for the partial flow case: again, the computational model only predicts an almost sudden drop in the performance. At overload condition, the simulations are in better agreement with the experiments: the drop of the performance curve is preceded by a noticeable increase of the head. However, the slope of the drop is still overestimated.

We may explain this inability of the simulation to predict a progressive decrease of the performance (prior to the complete blockage effect) by a late inception of the cavitation. Now, several simulations performed with different values for the empirical model coefficients such as the constants of vaporization and condensation, the volume fraction of incondensable, did not show significant differences in the head-drop curves.

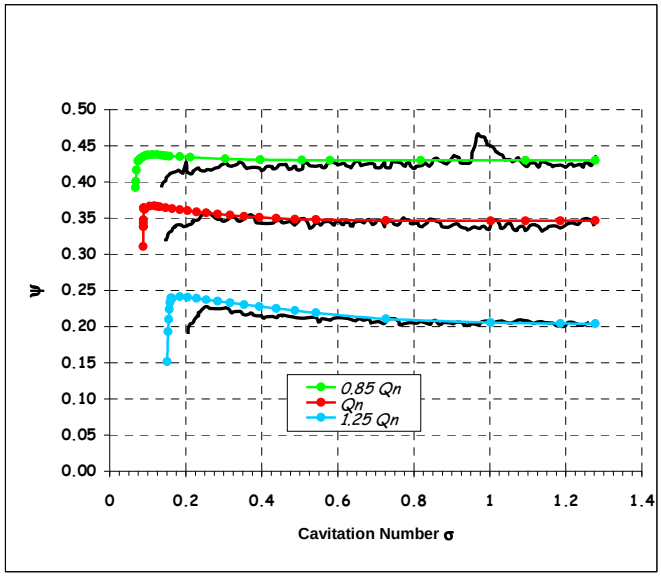

Figure 12: *Head-drop curves in cavitating conditions: comparison of supplied energy coefficients ψ at $0.85Q_n$, Q_n, $1.25Q_n$*

The figures [Fig. 13] compare the development of the cavitation pockets for different cavitation numbers, obtained in two solvers. All results were obtained with the same turbulence model (SST) and the same empirical values for the cavitation as well as the same convergence criteria described in the paragraph « *comments of numerical adjustments and turbulence model influence* ». Independently from the subtleties of coding, the numerical scheme of convective terms does influence the development of the cavitation pockets. The figures show that the schemes MPLS + PAC (velocities) and UDS (α_l) that are more diffusive, lead to pocket that are clearly more developed than the one predicted by Full BJ_MUSCL (velocities and α_l). However these differences do not have an effect on the Head-drop curves which remain almost similar

Figure 13 : $Q=Q_n$ – Numerical Results – (yellow) CFX10 – (Cyan) CFXTASCFlow

Visualization of Cavitation pocket - α_v = 0.1 - SS: Suction Side PS : Pressure Side

	σ = 0.1265	σ = 0.1320	σ = 0.1412	σ = 0.1430
SS	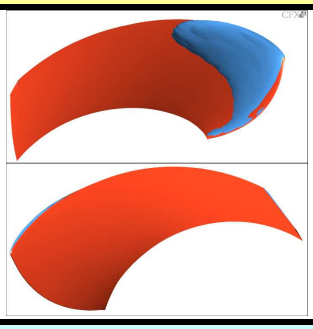	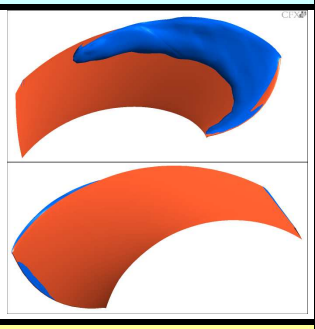	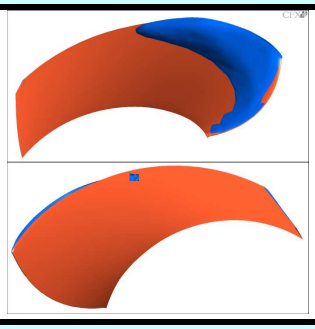	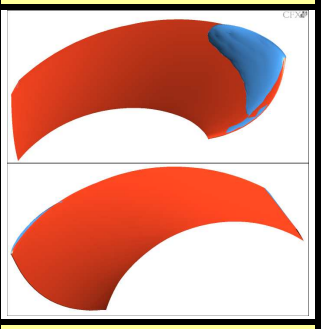
PS				
	σ = 0.1609	σ = 0.1669	σ = 0.1780	σ = 0.1265
SS	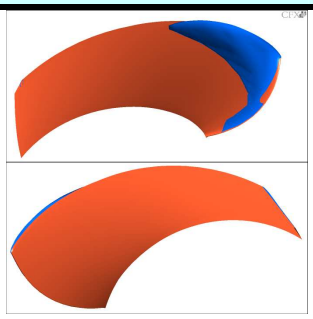	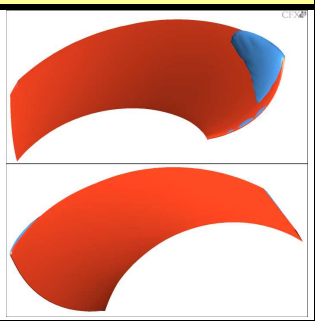	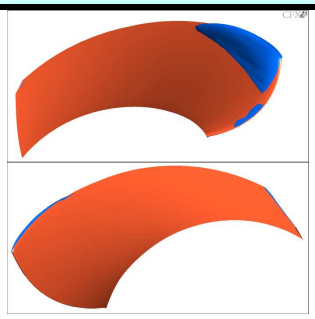	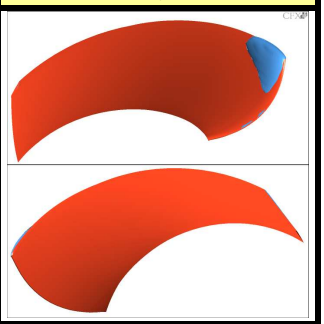
PS				

Figure 14a : $0.85Q_n$

Visualization of Cavitation pocket - α_v = 0.01 - SS: Suction Side PS : Pressure Side

	σ = 0.1236		σ = 0.1567	
	Numerical Results	Experimental Data	Numerical Results	Experimental Data
SS	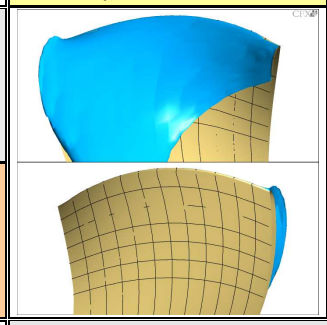	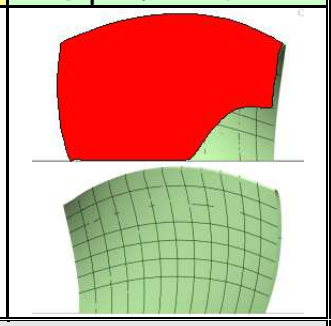	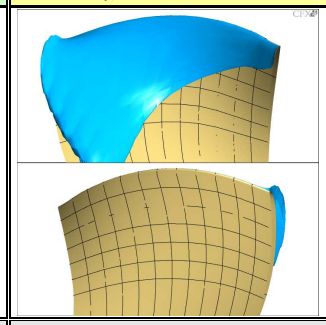	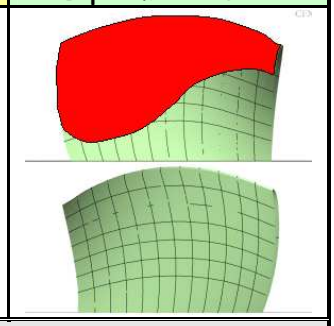
PS				
	σ = 0.2118		σ = 0.5059	
	Numerical Results	Experimental Data	Numerical Results	Experimental Data
SS	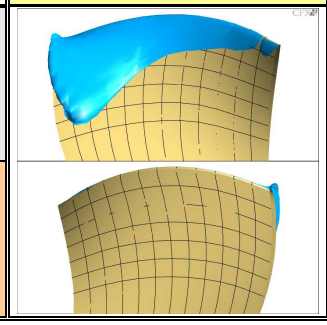	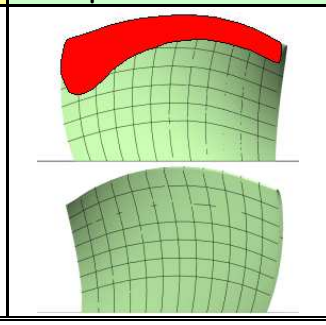	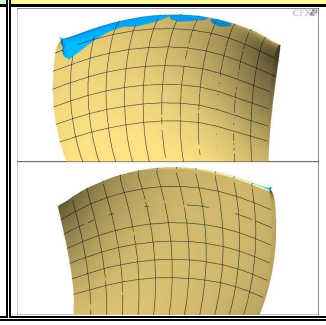	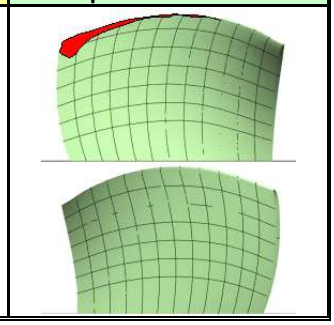
PS				

Figure 14b : Q_n

Visualization of Cavitation pocket - α_v = 0.01 - SS: Suction Side PS : Pressure Side

	σ = 0.2283		σ = 0.2835	
	Numerical Results	Experimental Data	Numerical Results	Experimental Data
SS	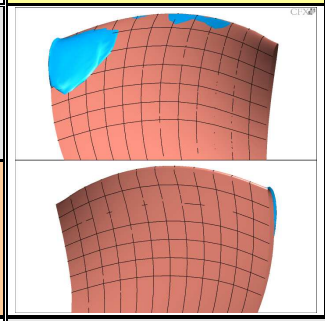	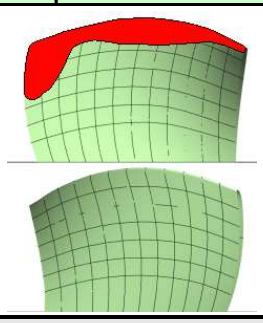	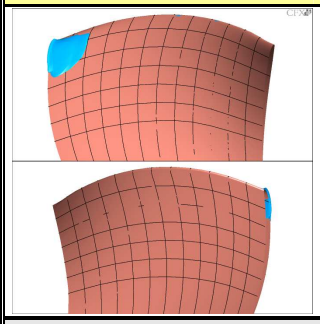	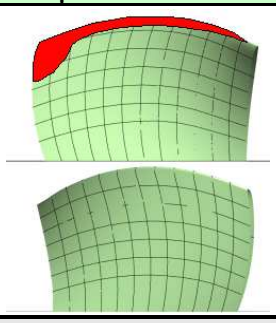
PS				

	σ = 0.3166		σ = 0.3938	
	Numerical Results	Experimental Data	Numerical Results	Experimental Data
SS	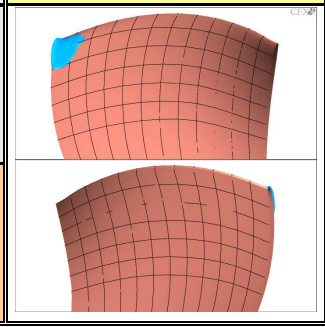	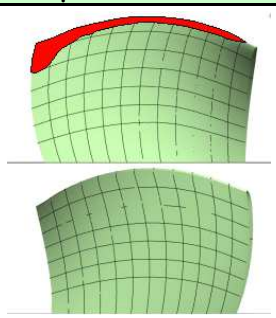	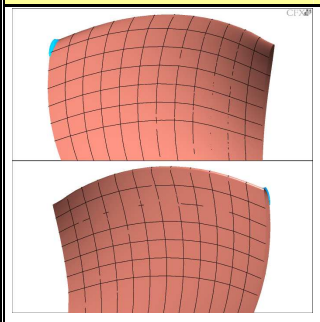	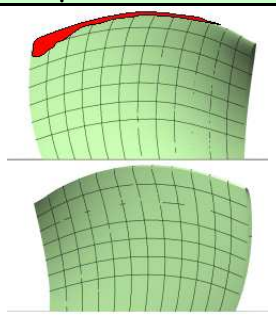
PS				

Figure 14c : 1.25 Q_n

Visualization of Cavitation pocket - α_v = 0.01 - SS: Suction Side PS : Pressure Side

	σ = 0.1843		σ = 0.2284	
	Numerical Results	Experimental Data	Numerical Results	Experimental Data
SS	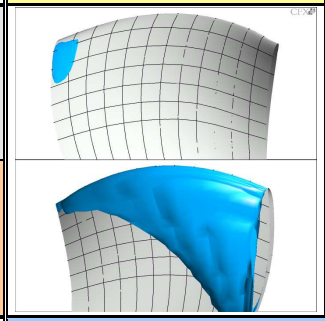	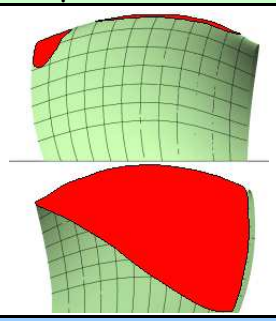	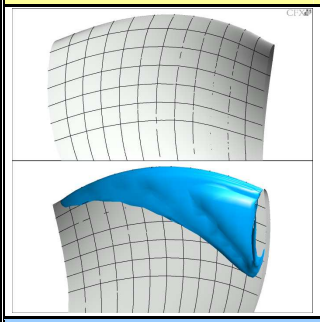	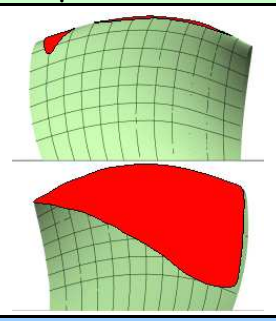
PS				

	σ = 0.2541		σ = 0.7264	
	Numerical Results	Experimental Data	Numerical Results	Experimental Data
SS	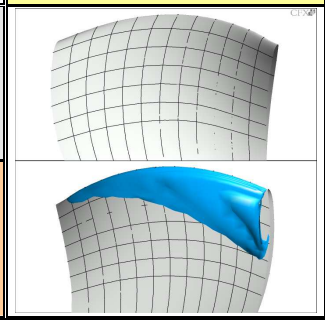	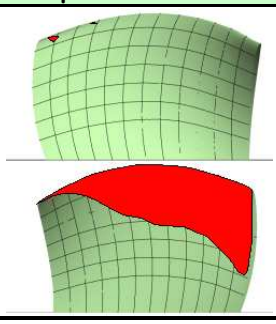	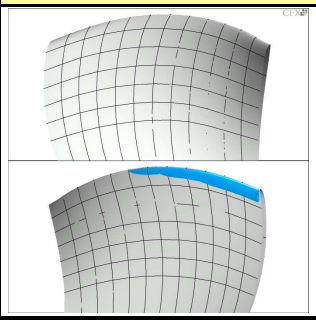	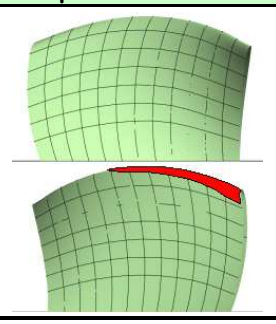
PS				

The figures [Fig. 14a, b, c] show the development of cavitation pockets observed in the blades and the ones predicted in CFX10. The threshold value used for the iso-surface that represents the cavitation pocket was set at α_v=0.01. A pressure coefficient distribution and volume fraction on the blade [Fig 17] indicates that this value remains representative of the cavity closure. The pocket developments near leading edge (surface and position of the cavity closure) are in very good agreement with the experiments.

At flow rate corresponding to 0.85 Q_n [Fig. 14a], the predicted shapes compare perfectly well with the ones observed for the pressure values from σ = 0.8 to the critical numerical value σ = 0.12. Still, this does not help to predict the beginning of the performance drop observed from $\sigma_d^{measured}$ = 0.28 ($\sigma_c^{measured}$ = 0.113). The mesh at the leading edge is not fine values of σ larger than 0.8.

At the nominal point [Fig 14b]; the comparison between testing and computation is not just as well. However, one observes that for values of σ larger than 0.39, an increase of the specific energy received by the fluid is consistent; this effect is most certainly related to the presence of cavitation pocket near the shroud. For values smaller than σ = 0.23 ($\sigma_d^{measured}$ = 0.23, $\sigma_c^{measured}$ = 0.14), this zone generates unstable bubble shedding. This unstable behaviour increases as the cavitation number decreases, leading to unstable detachment of the cavitation pockets along the line of closing. These phenomena can be the cause of the decrease of the performance observed before its fall. This is obviously not captured by our simulations in stationary regimes.

At overload condition [Fig 14c], the shapes and positions of pockets observed in experiments are quite correctly predicted for values of σ lower than 0.26 and approaching the computational critical value of σ = 0.16 One can observe that at values of flowrate above the nominal point, these pockets develop at the pressure side of blade. However, as for the partial flow case, this good agreement does not permit to predict the decrease of the performance that appears at ($\sigma_d^{measured}$ = 0.23 ($\sigma_c^{measured}$ = 0.2). One observes though that for these two regimes, the pockets have a stable behaviour. Some transient phenomena can be noticed but remain localized to the region of closure, which does not vary much with the extension of the pocket. This leads us to think that unlike for the nominal point, the performance drop is not caused by the unstable behaviour of the pockets but perhaps by an inadequate description of the boundary layer downstream the cavitation zone. For values of σ larger than 0.26, the increase of the energy received by the fluid is correctly reproduced by the simulation. One can notice though, that for values above 0.45, a slight difference appears in the extensions of the pockets; these differences can be related to the spatial definition of this zone.

The curves in figure [Fig. 15] give, for the 3 operating conditions, the evolution of the specific energy supplied by the impeller and of the specific energy transferred to the flow. These coefficients are divided by those obtained for the operating mode corresponding to the non-cavitating flow. The coefficients ($\sigma_d^{measured}$ are also reported on the curves: they correspond to the start of performance drop. In experiments, cavitation appears rapidly through stable pockets at quite high cavitation numbers: σ = 1.1 at 0.85Q_n, σ = 0.7 at Q_n, σ = 1.2 at 1.25Q_n.

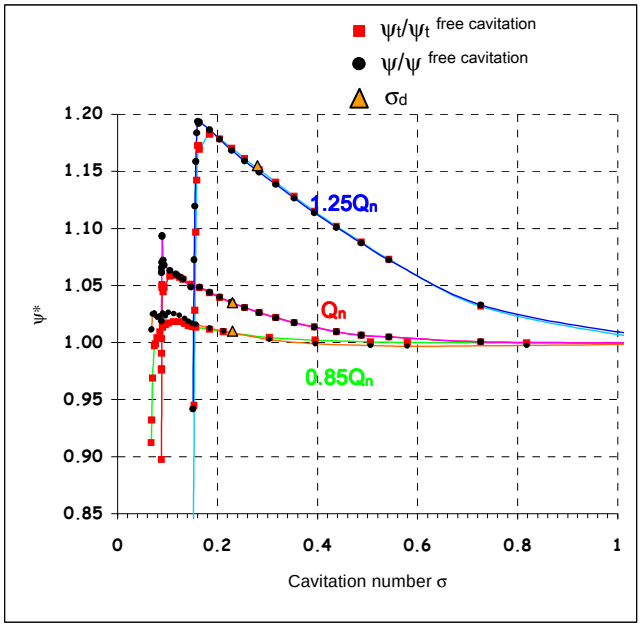

Figure 15 *Head-drop curves in cavitating conditions: comparison of supplied ψ and transferred energy coefficients ψ_t at 0.85Q_n, Q_n, 1.25Q_n*

When the cavity closure moves away from the blade edge, the specific energy coefficient increases from the following values: σ = 0.4 at 0.85Q_n, σ = 0.5 at Q_n, σ = 1.25 at 1.25Q_n. This phenomenon is mostly marked at overload condition for which pockets are more developed at high values of σ. Experimental and computational curves are in good agreement on reproducing this phenomenon up to critical values where, as already seen, one notes a performance drop at the following operating conditions: σ_d = 0.28 at 0.85Q_n, σ_d = 0.23 at Q_n, σ_d = 0.23 at 1.25Q_n, while simulations not only do not reproduce this trend, but even predict an increase of the head.

The figure [Fig. 17] gives the distribution of the pressure coefficient Cp along the blade chord for both 0.1 and 0.9 span values. The flow rate is equal to 1.25Q_n and cavitation conditions are: free cavitation, σ = 0.4, σ = 0.2 (before a breakdown) and σ = σ_b = 0.15. The pressure distribution on the blades is modified by cavitation: for σ = 0.4, 0.2. Compared to the case without cavitation, Cp decreases in the leading edge area and then increases at the cavity closure zone and increases again to the trailing edge.

The gain is higher than the loss, which increases the torque. At the point $\sigma_s = \sigma_b$, a cavitation pocket extends beyond the edge region and reaches the opposite side of the blade passage [Fig. 16]. The strong disturbance of the flow in this zone leads to lower value of the energy supplied to the fluid. A reduction of the pressure (i.e. cavitation number) means an extension of the cavitation pockets which could explain a loss in the torque [Fig. 17] and lead to a drop of specific supplied energy. However, we note that this supplied energy decreases faster that the transferred energy [Fig 15], which reveals that the hydrodynamic losses due to cavitation development plays a major role in the head drop phenomenon. This trend is particularly noticeable at the partial flow rate.

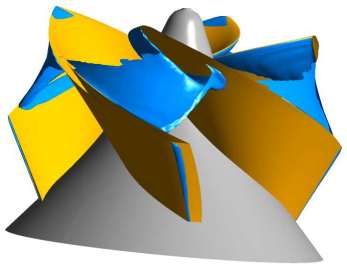

Figure 16: *Numerical prediction of cavitation pocket at 1.25 On and σ= 0.16*

An underestimation of the pressure level needed to trigger these phenomena, especially the cavitation pocket growing on the blade side in front of the leading edge, can explain the impossibility for the model to predict the development of the head drop experimentally observed for the partial flow and overload conditions. The mesh may be too much coarse to pick up the real deformation level of the flow due to the presence of pockets developing on the blade leading edges. Mesh density in near wall zones may be insufficient to correctly evaluate gradients, more particularly downstream the cavitation pockets. This can lead to an underestimation of the turbulence level and an overestimation of the wall pressure; it can explain the bad prediction of hydraulic losses before the breakdown and the pressure offset necessary to launch cavitation phenomena near the trailing edge.

The study of the non cavitating flow shows that flow rate assumed as the nominal one does not correspond to optimal one. This can account for the trend of this operating point to generate along leading edges very intense swirling structures that are able to amplify the dynamic observed alongside the cavity closure [Bachert et al, 2003], and thus unbalance the whole pocket near the shroud, considering a given entrance pressure. This unstable behaviour experimentally detected will be taken into account only if an unsteady flow simulation is performed. The volute can also act on pressure distribution on impeller outlet, what can first modify the torque and then the threshold value of cavitation number from which the cavitation pocket appears.

This explanation of the mechanism, bringing to experimental head drops and to the breakdown phenomenon for calculation, remains consistent with Bachert's interpretation [Bachert et al, 2003], except for the order of pocket development on pressure side and suction side depending on the operating point. In our case, the main cavitation pocket reaches the opposite side, located on the other end of the passage. For the 3 operating points carried out, no rotating cavitation phenomena have been experimentally visualized. This dismisses their influence on the head drop, they are generally observed for lower values of partial flow [Hoffmann et al, 2001].

CONCLUSION

CFD Simulation of the flows in the hydraulic turbo-machineries always obliges to find a compromise between smoothness of grid and precision necessary to correctly predict the included phenomena. For non-cavitating flow, the mesh grids usually used (200 000 to 300.000 nodes/passage) make it possible to obtain reliable results in particular to evaluate the performances of the pumps, if we don't move away too much from the nominal point. Indeed in this case, more complex flow structures can appear requiring to refine the grid and to extend the domain of calculation which will not be limited any more at only one passage but risk to extend to the whole pump, giving time consuming calculations. Moreover, to benefit from models of turbulence able to describe the boundary layer, the density of nodes will be likely to be high close to the walls. In the case of the simulation of cavitating flow, times calculations will be amplified, the more the non-linear behaviour of the model often obliges to under-relax the solver, in particular when one approaches the critical points.

The use of the cavitation model based on the VOF approach, of the first order approximation of the *Rayleigh-Plesset* equation, of a domain of calculation limited to only one passage and of a number of elements of discretization which ensures for a non cavitating flow an acceptable compromise between precision and CPU time (220 000 nodes), makes it possible to predict correct behaviour of the cavitating flow in the helico-centrifugal pump.

For the three operating conditions considered, simulations predict extents of cavitation pockets in conformity with those observed in experiments: position, size. The numerical results confirm that the cavitation zones located downstream from the leading edge and close to the shroud become unstable when the pressure of inlet corresponds to the experimental value where the head starts to decrease. The two codes used in this study, CFX-TASCflow and CFX10 give a quasi-similar evolution of the global performance. The first tends to over-estimate the

pocket development near leading edge, but this gives no significant effect for the head evolution.

The precision of evaluation of the convective terms plays a major part in the prediction of the pockets. The strategy used in CFX10 resting on Numerical Advection Correction respecting a multidimensional criterion of monotony seems more effective than that based on the scheme MPLS + PAC. This last is in addition only applied to the momentum apart from the zones of cavitation. It shows that the migration for this type of study to-wards CFX10 (CFX11) is relevant, the more so as this gain of precision can become capital during non stationary simulations, in condition however of reformulating the evaluation of turbulent viscosity and of the threshold pressure of the cavitation model. Because, in the contrary, we can artificially stabilize the pockets of cavitation. The use of grids based on hexahedral elements remains preferable. In the same order, the expansions and the deformations of mesh must remain moderate. Because in the contrary case, the evaluation of the gradients of the node center will be able to degrade the gain of precision brought by the corrective term. And this degradation will be all the more significant on a skewed element if the criterion of monotony is applied to all the contributions of the corrective term of the scheme.

The calculations make it possible to reproduce the extent of the pockets and the increase head observed in experiments, during the reduction of the inlet pressure. This phenomenon corresponds to a modification of the pressure distribution downstream from the cavitation pockets. However, they do not succeed in predicting the appearance of the measured head-drop. Calculations continue to predict an increase in head, until the quasi simultaneous fall of head and torque. This phenomenon of quasi breakdown appears when the cavitating zone enlarges and reaches an opposite side of the adjacent blade. From the impeller geometry, this area is near of the outlet of the passage. One reason not making possible to predict the head-drop correctly, can be due to a pressure level too much low compared to the tests to initiate such a phenomenon.

Before prospecting towards more advanced models: physical model take in account the water quality (full cavitation model), leakage flow and influence of the casing, we must first check that a better description of the boundary layer in this zone: meshing and model, can correct this delay. The instationary behaviour observed at the nominal flow rate will have to be also taken into account. In a general way, the refinement of the mesh will lead towards numerical difficulties obliging to simulate in a non stationary mode the flow in the complete impeller!

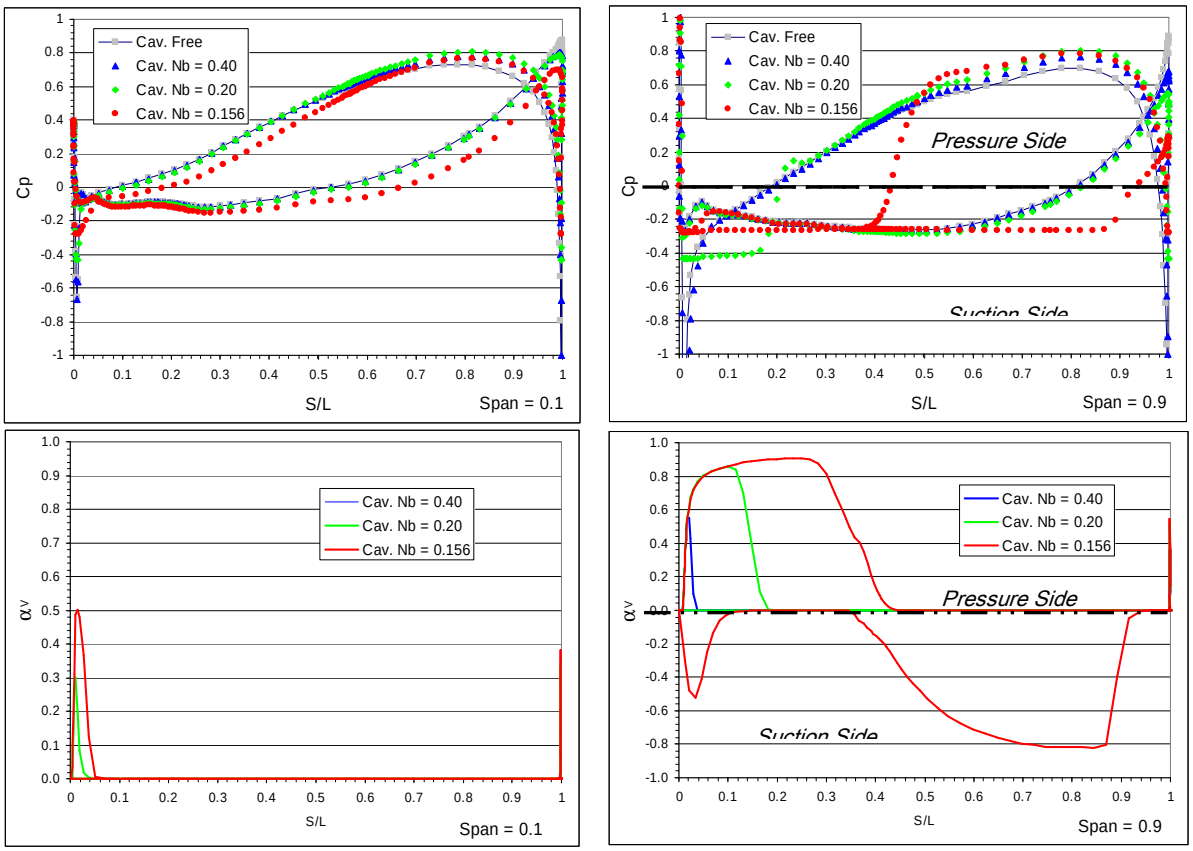

Figure 17: *Evolution of Cp coefficient and vapor volume fraction on the balde near the hub and the shroud areas at 1.25 Qn and free cavitation, σ=0.2 and σ=0.156*

ACKNOWLEDGMENTS

We would like to thank Guido Doebbener, ANSYS inc., Otterfing, Germany for his collaboration during the project.

REFERENCES

AEA Technology Engineering Software. CFX-Tascflow Computational Fluid Dynamics Software, Documentation Version 2.12, 2002.

ANSYS-CFX, Release 10.0, Computational Fluid Dynamics Software, Solver Guide, 2005.

Ait Bouziad y, Guennmoun F., Farhat M., Avellan F., Numerical Simulation of Leading Edge Cavitation, Proceedings of FEDSM'03 4th ASME-JSME Joint Fluids Engineering Conference, July 6-11, Honolulu, Hawaii, USA, 2003.

Ait Bouziad y, Farhat M., Guennmoun F., Kueny J.L., Avellan F., Physical Modelling and Simulation of Leading Edge Cavitation, Application to an Industrial Inducer, Fith International Symposium on Cavitation, November 1-4, Osaka, Japan, 2003.

Ait Bouziad Y., Farhat M., Kueny J.L., Avellan F., Miyagama K., Experimental and numerical cavitation flow analysis of an industrial inducer. 22nd IAHR Symposium on Hydraulic Machinery and Systems, June 29 – July 22, Stockholm, Sweden, 2004

Ait Bouziad Y., Physical modelling of leading edge cavitation: Computational methodologies and application to hydraulic machinery. PhD thesis, Ecole Polytechnique Fédérale de Lausanne, 2006 (N°3353)

Asuaje M, Bakir F., Kouidri S., Kenyery F., Rey R., Numerical Modelization of the Flow in Centrifugal Pump:Volute Influence in Velocity and Pressure Fields, International Journal of Rotating Machinery 3:244-255, 2005.

Athavale M.M, Li H.Y., Jiang Y., Singal A. K., Application of the full cavitation model to pumps and Inducers, International Journal of Rotating Machinery, 8: 45-56, 2002.

Bache G., Thomas M., Validation an Efficient and Accurate Turbomachinery CDX Analysis Procedure, in 28th Aerospace Sciences Meetings, AIAA Paper 98-681, January 8-11, 1990.

Bachert R., Ludwig G., Stoffel B., Frobenius M., Schilling R., Three-Dimensional Unsteady Cavitation Effects on a Single Hydrofoil and in a Radial Pump-Measurements and Numerical Simulations, Fith international Symposium on Cavitation, November 1-4, Osaka, 2003.

Bakir F., Mejeri I., Kouidri S., Rey R., Hub Shape Effects under Cavitation on the Induceurs Performance, Fith International Symposium on Cavitation, November 1-4, Osaka, 2003.

Bakir F., Rey R., Gerber A.G., Belramri T., Hutchinson B., Numerical and Experimental Investigations of the Cavitating Behavior of an Inducer, The International Journal of Rotating Machinery, Volume 10, Number 1 / Jan-Feb, 2004.

Barth T.J., Jespersen D.C., The Design and Application of Upwind Schemes on Unstructured Meshes,. AIAA Paper 89-0366, P 1-12, 1989.

Barth T.J., *Numerical Methods for Conservation Laws on Structured and Unstructured Meshes,* 33rd Computational Fluid Dynamics Course – Novel Methods for Solving Convection Dominated Systems, VKI March 2003.

Basuki W., Schnerr G.H., Yuan W., Single-Phase and Modified Turbulence Models for Simulation of Unsteady Cavitating Flows, Wissenschaftliche Berichte FZKA, 6759:F.14-F.29, 2003.

Catelan F.X., Ouaabi A., Cavitation dans une roue centrifuge (Pompe Volute béton) à l'auide du logiciel TASC-Flow 2.12 et comparaison avec les résultats expérimentaux, Proceedings de la 164ème session du Comité Scientifique et Technique SHF, Colloque d'Hydrotechnique, 7 avril, Chatou, France, 2005.

Combes, J.F., Archer, A., Etude de l'érosion de cavitation dans la pompe SHF, Proceedings de la 164ème session du Comité Scientifique et Technique SHF, Colloque d'Hydrotechnique, 21-22 Novembre, Chatou, France, 2000.

Coutier-Delgosha O., Astolfi J.A., Numerical Prediction of The Cavitating Flow on a Two-Dimensional Symmetrical Hydrofoil with a Single Fluid Model, Fith International Symposium on Cavitation, November 1-4, Osaka, Japan, 2003.

Coutier-Delgosha O., Fortes-Patella R., Hofmann M., Stoffel B., Experimental and Numerical Studies in a Centrifugal Pump With Two-Dimensional Curved Blades

in Cavitating Condition, Journal of Fluids Engineering, 125:970-978, 2003

Coutier-Delgosha O., Morel P., Fortes-Patella R., Reboud JL., Numerical Simulation of Turbopump Inducer Cavitating Behavior, Int. Journal of Rotating Machinery, 2:135-142, 2005.

Darwish M.S, Moukalled F., *TVD Schemes for Unstructured Grids*, Int. Journal of Heat and Mass Transfer, 4:599-611, 2003.

Ferry M., Piquet J., Evaluation of a new fully coupled method for the solution of Navier Stokes equations, Proc . 3rd. European Multigrid Conference, Bonn. GMD Report, Trottenberg, Ed 1991.

Franc J.P., Rebattet C., Coulon A., An Experimental Investigation of Thermal Effects in a Caviting Inducer, Journal of Fluids Engineering, 126:717-723, 2004.

Friedrichs J., Kosyna G., Unsteady PIV Flow Field Analysis of a Centrifugal Pump Impeller Under Rotating Cavitation, Fith International Symposium on Cavitation, November 1-4, Osaka, Japan, 2003.

Gros L., Pierrat D., Pintrand G., Ferry M., Implémentation du solveur couplé Migal dans code Saturne, Rapport CETIM, 1N8331, 2006.

Hanjalic K., Will RANS Survie LES? A View of Perspectives, Journal of Fluids Engineering, 127:831-839, 2005.

Hirschi R., Dupont Ph., Avellan F., Favre J.N., Guelich J.N., Handloser W., Parkinson E., Centrifugal Pump Performance Drop due to Leading Edge Cavitation:Numerical Predictions compared with Model Tests, Journal of Fluids Engineering, 120: 705-711, 1998.

Hosangadi A., Ahuja V., A New unsteady Model for Dense Cloud Cavitation in Cryogenic Fluids, Proceedings of FEDSM2005, June 19-23, Houston, TX, USA, 2005.

Hoffman M., Stoffel B., Coutier-Gelgosha O., Fortes-Patella R., Reboud JL., Experimental and Numerical Studies on a Centrifugal Pump with 2D-Curved Blades in Cavitating Condition, Fourth International Symposium on Cavitation, June 20-23-4, Pasadena, California, USA, 2001.

Hoffman M., Stoffel B., Friedrichs J., Kosyna G., Similarities and Geometrical Effects on Rotating Cavitation in Two Scaled Centrifugal Pumps, Fourth International Symposium on Cavitation, June 20-23-4, Pasadena, California, USA, 2001.

Hutchinson B.R., Raithby G.D., A Multigrid Method Based on the Additive Correction Strategy, Numerical Heat Transfer 9:511-537, 1986.

Hutchinson B.R., Galpin P.F., Raithby G.D., Application of additive correction multigrid to the coupled fluid flow equations, Numerical Heat Transfer 13:133-147, 1988.

Kawamura T., Sakoda M., Comparison of Bubble and Sheet Cavitation Models for Simulation of Cavitating Flow Over A Hydrofoil, Fith International Symposium on Cavitation, November 1-4, Osaka, Japan, 2003.

Luo X., Nishi M., Yoshida K., Dohzono H., Miura K., Cavitation Performance of a Centrifugal Impeller Suitable for a Mini Turbo-Pump, Fith International Symposium on Cavitation, November 1-4, Osaka, Japan, 2003.

Mejeri I., Bakir F., Rey R., Experimental and Numerical Analysis of Unsteady Cavitation Instabilities in an Axial Inducer, Sixth International Symposium on Cavitation, September 11-15, Wageningen, Netherlands, 2006

Mejeri I., Bakir F., Rey R., Comparaison of Computational Results Obtained From a Homogeneous Cavitation Model With Experimental Investigations of Three Inducers, Journal of Fluids Engineering, 128:1308-1323, 2006

Menter F.R., Influence of free stream values on k-w turbulence model predictions, AIAA-Journal, 30:1657-1659, 1992.

Menter F.R., Zonal Two Equation k-w Turbulence Models for Aerodynamic Flows, in 24th Fluid Dynamics Conference, AIAA Paper 93-2906, july, Orlando, 1993.

Menter F.R., Two-equation eddy-viscosity turblence models for engineering applications, AIAA-Journal, 32:269-289, 1994.

Menter F.R., A Comparison of Some Recent Eddy-Viscosity Turbulence Models, Journal of Fluids Engineering, 118:514-519, 1996.

Pierrat D, Gros L., Pintrand G., Numerical Advection Correction Schemes, Rapport CETIM, To appear

Pouffary B., Fortes-Patella R., Reboud JL., Numerical Simulation of Cavitating Flow around a 2D Hydrofoil: A barotropic Approach, Fith International Symposium on Cavitation, November 1-4, Osaka, Japan, 2003.

Raithby G.D., Skew Upstream Differencing Schemes for Problems Involving Fluid Flow, Computationals Methods for Applied Mechanical Engineering, 9:153-164, 1976.

Raw M., A new control-volume-based finite element procedure for the numerical solution of the fluid flow and scalar transport equations, Doctoral Thesis, University of Waterloo, Ontario, Canada, 1985.

Raw M., Robustness of Coupled Algebraic Multigrid for the Navier-Stokes Equations, AIAA 96-0297, 1996.

Reboud JL., Coutier-Delgosha O., Pouffary B., Fortes-Patella R., Numerical Simulation of Unsteady Cavitating Flows Some Applications and Open Problems, Fith International Symposium on Cavitation, November 1-4, Osaka, Japan, 2003.

Ruge, J. and Stüben, K., Multigrid Methods, In. McCormick, S.F, Editor, Algebraic Multigrid, Frontiers in Applied Mathematics. Society for Industrial and Applied Mathematics, Philadelphia, Pennsylvania, U.s.A., 1987.

Saito Y., Nakamori I., Ikohagi T., Numerical Analysis of Unsteady Vaporous Cavitating Flow around Hydrofoil, Fith International Symposium on Cavitation, November 1-4, Osaka, Japan, 2003.

Scheuerer G., Development and Validation of a Cavitation Model in CFX5, Proceedings de la 164ème session du Comité Scientifique et Technique SHF, Colloque d'Hydrotechnique, 7 avril, Chatou, France, 2005.

Schneider G.E., Raw M., A Skewed, Positive Influence Coefficient Upwinding Procedure for Control-Volume-Based Finite-Element Convection-Diffusion Computation, Numerical Heat Transfer 9:1-42, 1986.

Schneider G.E., Raw M., Control Volume Finite-Element Method for Heat Transfer and Fluid Flow Using Colocated Variables-1 Computational Procedure, Numerical Heat Transfer 4:363-390, 1987

Schneider G.E., Raw M., Control Volume Finite-Element Method for Heat Transfer and Fluid Flow Using Colocated Variables-2 Application and Validation, Numerical Heat Transfer 4:363-390, 1987

Singhal A.K., Athavale M.M., Yang H.Q., Recent advances (Ventilated Cavitation) with the Full Cavitation Model, Eccomas 2004, Jyväskylä, July 24-28, 2004.

Wilcox D.C, Turbulence Modeling for CFD, DCW Industries, Inc., La Canada, CA, 1993.

Yang H.Q., Shinghal A.K., Megahed M., The Full Cavitation Model, VKI, Lecture Series 2005-04, Industrial Two-Phase Flow CFD, May 23-27, 2005.